Raman Spectra of Ionic Liquids: A Simulation Study of AlF_3 and Its Mixtures with NaF

Zehra Akdeniz[†] **and Paul A. Madden***[,‡]

Department of Physics, Istanbul University, Istanbul, Turkey, and Chemistry Department, Edinburgh University, The King's Building, West Mains Road Edinburgh EH9 3JJ, U.K.

Received: January 4, 2006; In Final Form: February 15, 2006

Theoretical Raman spectra of the melts of NaF/AlF_3 mixtures have been obtained from computer simulations in order to examine how the Raman spectra reflect the coordination structure around the Al^{3+} ions. The Raman spectra, both polarized and depolarized, are calculated from a model for the dependence of the polarizability of the system on the ionic coordinates which was inspired by electronic structure calculations of the polarizabilities of ions in a condensed-phase environment. The shapes of the spectra and their evolution with composition in the mixtures conform remarkably well to those seen experimentally, and we discuss the relationship between the bands seen in the spectra and the vibrational modes of the $AlF_n^{(3-n)}$ coordination complexes which are found in the melts. Finally, we calculate quantities which relate to the degree of cross-linking between these coordination complexes and their lifetimes.

I. Introduction

In recent papers,[1,2] it has been shown how it is possible to simulate the Raman spectra of moderately complex molten salts. A model for the dependence of the fluctuating polarizability of the melt on ionic positions, which had been suggested by electronic structure calculations,[3,4] was combined with a polarizable interaction potential,[5] refined on the basis of structural studies. For $LaCl_3$ and $ScCl_3$, which might be regarded as representatives of a broad class of trivalent metal halides[6−8] (with La^{3+} being a large cation and Sc^{3+} comparatively small), we obtained semiquantitative agreement with experimental spectra[9,10] for the pure melts and their mixtures with NaCl and CsCl. This development opens up the prospect of quantitative interpretation of such Raman spectra, which have, for many years, offered the most widely studied window onto the microscopic structure of these melts. The simulations offer a way of bridging an interpretative gap between the structure as seen spectroscopically, where attention focuses on the coordination complexes responsible for the discrete Raman bands, as in a molecular system, and in diffraction experiments, where the data is discussed from a more atomistic perspective in terms of radial correlations in an ionic mixture.[7,8] A further prospect is to relate the insights into the local structures in the melts, gained from spectroscopy and diffraction, to the transport properties of the melts.[11]

Apart from the intrinsic interest in completing these links, melts of the general composition MX_3/AX (where M is a trivalent metal, X a halogen, and A an alkali) are of interest in a number of electrochemical technologies.[12,13] Molten cryolite (Na_3AlF_6 or $AlF_3/3NaF$) is a stoichiometric compound in a continuous range of liquid $AlF_3/(NaF)$ solutions, which has special interest because of its role in the industrial Hall−Heroult process[12] for the electrodeposition of Al metal from alumina. There are no neutron or X-ray diffraction data to allow a direct determination of the coordination environment of the Al^{3+} ions due to the high melting temperature and consequent difficulties of sample containment. However, extensive Raman measurements have been made, by Gilbert and co-workers[14,15] in particular, and have provided the working model for the way that the mixture composition affects the coordination structure. As we will discuss at length below, the composition dependence of the band structure observed in the cryolite Raman spectra differs qualitatively from that seen in the MCl_3/ACl systems mentioned above, so it is a challenge to see if, with similar simulation methods to those used in chloride work, we can recover the cryolite data and explain why the fluoride and chloride spectra should differ in this way. In addition to the Raman work, recent pioneering high-temperature NMR measurements[20] have given information on the evolution of the coordination environment with the melt composition. The fact that neither technique *directly* measures structure makes simulation work useful in underpinning the interpretation of these measurements. The development of a simulation model which can reproduce the available experimental data will be very useful for modeling processes directly relevant to the electrochemical extraction process inter alia, such as the activity coefficients of the ions present and diffusion in the vicinity of the electrochemical interface.

In discussing the coordination structure of polyvalent cations in alkali halide solutions, it has often been presumed that the cation will have a preferred coordination number for a given anion determined, in large part, by the ratio of the cation to anion ionic radii. For Al^{3+}/F^-, it might be assumed that this preferred number is 6, based upon the crystal structures of AlF_3, $Na_5Al_3F_{14}$ (chiolite), and Na_3AlF_6 (cryolite), and that this would be the coordination number in molten AlF_3/NaF mixtures at low AlF_3 concentration where there are sufficient F^- ions to complete the coordination shell without sharing. Such melts could therefore be described as containing independent AlF_6^{3-} ions dispersed in a "solvent" consisting of Na^+ ions and excess F^-; this expectation seems to be broadly consistent with the experimental data (and the simulations described below). If we then move to mixtures more concentrated in AlF_3—beyond the $AlF_3/3NaF$ composition so that there are insufficient F^- ions for each Al^{3+} to complete its coordination shell with six

[†] Istanbul University.
[‡] Edinburgh University.

10.1021/jp060064h CCC: $33.50
Published on Web 03/16/2006

members—there are two possible limiting scenarios. Either the coordination number is retained with F^- ions being shared between the coordination shells of different cations (to form corner- or edge-sharing linkages between coordination complexes) or the coordination number drops to allow a higher degree of independence between them. If the coordination number dropped to 4, for example, then even the relatively concentrated mixture of AlF_3/NaF could consist of independent AlF_4^- and Na^+ ions.

Broadly speaking, the Raman spectra suggest that the first scenario is adopted in the MCl_3/ACl mixtures, since the Raman band structure is similar across a wide range of compositions,[16,2] whereas the AlF_3/AF mixtures exhibit more pronounced changes of coordination numbers with changing composition. In particular, Gilbert and co-workers[14,15] have proposed that, in the melts of $NaAlF_4$, the only significant aluminum-containing species is the tetrahedral AlF_4^- ion. The most direct evidence for this is the four line Raman spectrum with the polarization characteristics expected for a tetrahedral molecule. The strong polarized band occurs at a frequency of 622 cm^{-1}, essentially the same as the symmetric stretching frequency observed for the $NaAlF_4$ gaseous molecule.[17] The continued presence of the 622 cm^{-1} band at lower AlF_3 mole fractions together with a band at 560 cm^{-1} and a shoulder at 510 cm^{-1} in the polarized Raman spectrum is taken to mean that three aluminum-containing species are present in the Na_3AlF_6 melt (cryolite). Gilbert assigns the liquid 560 cm^{-1} band to AlF_5^{2-} and the 510 cm^{-1} band to AlF_6^{3-} because of the way the relative intensity of these features changes with composition. This assignment suggests that five-coordinate aluminum is by far the dominant environment in liquid Na_3AlF_6. Controversies about this assignment[18] have been resolved in recent work.[19] The predominance of AlF_5^{2-} in molten cryolite is consistent with the NMR data.[20,21]

We begin by describing the development of an interaction potential for cryolite and reviewing the background to the calculation of the Raman spectrum. We have calculated Raman spectra across the range of compositions from $NaAlF_4$ to Na_3AlF_6 and simultaneously studied the structure and dynamics of the coordination complexes of the cryolitic melts. Using the methods introduced by Pavlatou et al.,[22] we will link the Raman bands to normal modes of vibration of the coordination complexes. Comparatively little progress has been made in relating the *depolarized* Raman spectra of the melts to the microstructure.[9,16] The depolarized bands are much broader and less well-defined than the isotropic ones. One of the key questions to be answered is which of the four mechanisms which contribute to the polarizability fluctuations is most significant for the depolarized spectrum. We will show that the depolarized spectra from the simulations evolve with concentration in a very similar way to the experimental ones and attempt to relate them to vibrations of the coordination complexes in the same manner as the isotropic spectrum. In the final section, we describe some information on the structure of the coordination complexes and their lifetimes which is straightforward to extract from the simulations but impossible to measure experimentally.

II. Expressions for the Raman Spectrum

The theory of the calculation of the Raman spectrum was discussed at length in ref 1, and here, we simply recapitulate the key points. The light scattering spectrum[16,23,24] for the scattering geometry characterized by the scattering vector **q** and where the polarizations of the incident and scattered radiation are the Cartesian directions *b* and *a* is proportional to the spectrum of the correlation function of the **q**th spatial Fourier component of polarizability density of the system, Π_{ab}, that is

$$I_{ab}(\mathbf{q},\omega) \propto Re\int_0^\infty dt e^{i\omega t}\langle \Pi_{ab}(\mathbf{q},t)\,\Pi_{ab}(\mathbf{q},0)^*\rangle \qquad (2.1)$$

For an ionic material, we[3,4] distinguish four contributions to the polarizability:

$$\Pi_{ab} = \Pi_{ab}^{SR} + \Pi_{ab}^{\gamma} + \Pi_{ab}^{B} + \Pi_{ab}^{DID} \qquad (2.2)$$

The terms Π_{ab}^{B} and Π_{ab}^{γ} represent the changes in the anion polarizability by hyperpolarization via the interionic Coulomb field, where *B* and γ are the dipole−quadrupole and dipole−dipole−dipole hyperpolarizabilities of the ion.[25] Π_{ab}^{DID} is the contribution due to first-order dipole-induced dipole effects, and Π_{ab}^{SR} is that due to the changes in the polarizability α_{ab}^{i} of an anion by the compression and deformation of the ion by its short-range interactions with its neighbors.[4,26] Detailed expressions for these different polarizability mechanisms in terms of the ionic coordinates are given in the Appendix (see also refs 1, 3, and 4), as well as values for the implicit parameters used in the present simulations.

The light scattering spectrum of an ionic system is thus quite complicated, as four mechanisms, with different dependencies on the interionic separations, can be expected to contribute. As discussed in the Introduction, the primary interest is in the isotropic spectrum, which reflects fluctuations in the trace of the polarizability density

$$\Pi_I \equiv \Pi_{xx} + \Pi_{yy} + \Pi_{zz} \qquad (2.3)$$

and dominates the polarized spectra. It can be shown that only the short-range (Π^{SR}) and gamma (Π^{γ}) mechanisms contribute to the trace of Π, due to the traceless nature of the dipole−dipole interaction tensor and the Coulomb field gradient. The isotropic spectrum can thus be regarded as the sum of three terms, the spectra of the autocorrelation functions of Π_I^{SR} and Π_I^{γ}, which we call the SR and γ "subspectra", as well as the spectrum of their cross-correlation function. As we discuss in the Appendix, we are not currently able to obtain the parameters which determine the amplitude of the SR polarizability fluctuations with any certainty, although the functional dependencies of the polarizabilities on the interionic separations should be reasonably reliable (as judged from their representation of ab initio information for simpler systems). Consequently, although the frequency dependencies of the subspectra should be reliable, we do not know how to combine them and the cross term to produce a total spectrum in which the different mechanisms are properly weighted. We will therefore only present results for the individual subspectra; since the relevant polarizabilities depend on the interionic coordinates in different ways, it might be expected that they would reflect different aspects of the dynamics of the melt which we would like to expose. This problem is even more pressing for the depolarized spectrum which will, in general, be affected by all four mechanisms; again, we will only discuss the subspectra.

The depolarized subspectra of the melt may be calculated from any one of the five independent anisotropic components of Π, such as Π_{xy}. As we discussed in ref 1, it is possible to calculate reasonably noise free depolarized subspectra for the melts by averaging over the spectrum of $\Pi_{ab}(\mathbf{q}=\mathbf{0})$ for these five independent components. For the isotropic spectrum, no such averaging is possible and we have again calculated spectra at the smallest values of *q* accessible in the simulation and

exploited the projection method, introduced in ref 1 to get spectra of the quality reported below.

III. Details of the Simulations

The simulations were carried out with polarizable ion interaction potentials, as described elsewhere.[5,27] A potential[28,29] has been devised for NaF/AlF_3 mixtures which reproduces the known crystal structures of compounds of stoichiometry AlF_3, $NaAlF_4$, $Na_5Al_3F_{14}$ (chiolite), and Na_3AlF_6 as well as the structures of a number of gas-phase species which had been calculated by ab initio methods. These crystal structures are nontrival, and polarization effects are found to play an important role in stabilizing them. The potentials have been used to study the vibrational frequencies of the isolated $MAlF_4$ molecules (M = alkali ion) and also of the solid compounds. The vibrational frequencies are in good accord with experimental spectra[17] in both cases, though the calculated frequencies for the stretching of Al−F bonds are higher than those found experimentally. The potential has now been used in simulations of the melts over the range of the compositions Na_3AlF_6, $Na_5Al_3F_{14}$, and $NaAlF_4$. The particular parameters used in the calculations have been refined somewhat from those used in the previous works.[28] As we wish to compare results for solutions of varying composition, we decided to simulate all of the systems at the same (zero) pressure. Before beginning then, we made small adjustments to the interaction potentials so that the pure melts (AlF_3 and NaF) had the correct molar volume[30] at 1300 K and zero pressure and the mixtures were close to the experimental densities.[31] The new potential parameters are given in the Appendix. Only the F^- and Na^+ ions are treated as being polarizable; the polarizability of Al^{3+} is tiny. The values for the ionic polarizabilities and short-range damping parameters[27] are also given in the Appendix.

The calculations were carried out at temperatures close to the melting point, 1250 K. We followed the same protocol for all simulations. All of the runs contained between 500 and 600 ions, depending on stoichiometry. We carried out a 100 000 step equilibration run (36 ps) in an NPT ensemble, using the integration algorithm suggested by Martyna et al.;[32] in all cases, the system settled to a density close to the experimental one[31] (typically about 2% larger). We then performed a 500 000 step NVT run, at the cell volume to which the system had equilibrated at zero external pressure, during which time correlation functions, and so forth, were calculated. Ewald sums were used for all Coulomb and multipolar interactions.[33] For the runs at lower temperatures, we have checked the systems have not crystalized and all compositions are still liquidlike by checking the diffusion coefficients.

IV. Simulated Raman Spectra of NaF/AlF_3 Mixtures

In Figure 1, we show a snapshot of the ionic positions taken from the simulation at the chiolite composition ($Na_5Al_3F_{14}$) and at 1350 K. F^- ions are shown in red, Al^{3+} ions in blue, and Na^+ ions in gray. Lines indicate "bonds" between Al and F ions if they are separated by less than the first minimum in the radial distribution function. The snapshot indicates that at this composition the melt contains four-, five-, and six-coordinated Al species. In this section, we will examine how they contribute to the features observed in the Raman spectrum.

A. Isotropic Spectrum. We begin by describing the isotropic spectra calculated from the MD runs at 1350 K. As discussed above, we show the subspectra associated with the SR and γ polarizability mechanisms separately in the upper panels of Figures 2 and 3, respectively. Contrary to the expectation that,

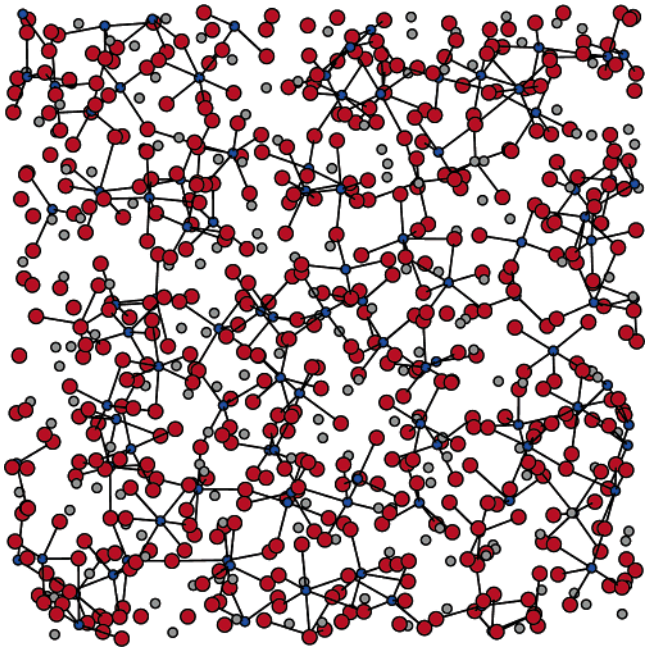

Figure 1. Snapshot of the ionic positions in a simulation of the chiolite composition ($Na_5Al_3F_{14}$). The F^- ions are shown in red, the Al^{3+} in blue, and the Na^+ in gray. Bonds are drawn between Al^{3+} and F^- ions which are closer than 4.8 au.

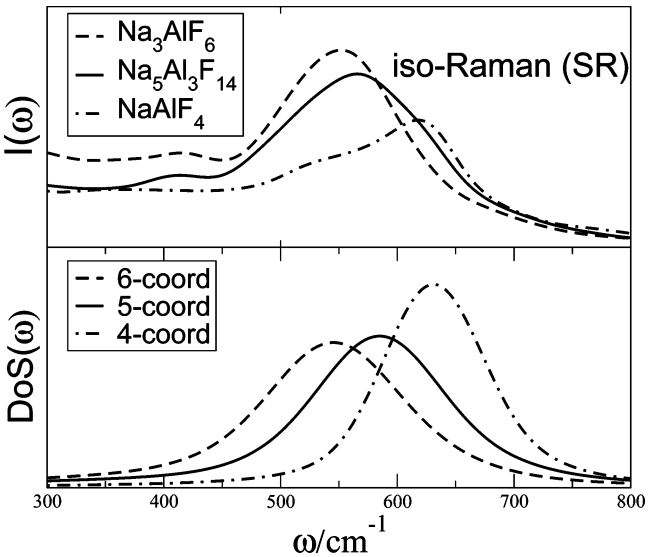

Figure 2. Isotropic Raman spectra (in the top panel) calculated for the short-range (SR) mechanism at three different melt compositions compared with the density of states (DoS) of the symmetric breathing vibrations of four-, five-, and six-coordinate complexes.

because of the very different dependencies of the underlying polarizabilities on the interionic coordinates, these subspectra would have different shapes, in fact, we see that they are broadly similar, meaning that both mechanisms pick up the same aspects of the ion dynamics in the melt. Both show a broad main band in the 500−700 cm^{-1} frequency window, which shows a pronounced shift toward higher frequencies as the composition of the mixture becomes richer in AlF_3, together with a weaker feature at about 400 cm^{-1}. As we will show in detail below, the main bands may be associated with symmetric breathing vibrations of the Al-centered coordination complexes. That this band shows a substantial dependence on the composition of the melt is an appreciable point of departure from our previous work on chloride melts, where, in agreement with the experimental observations, the band retained a similar shape and central

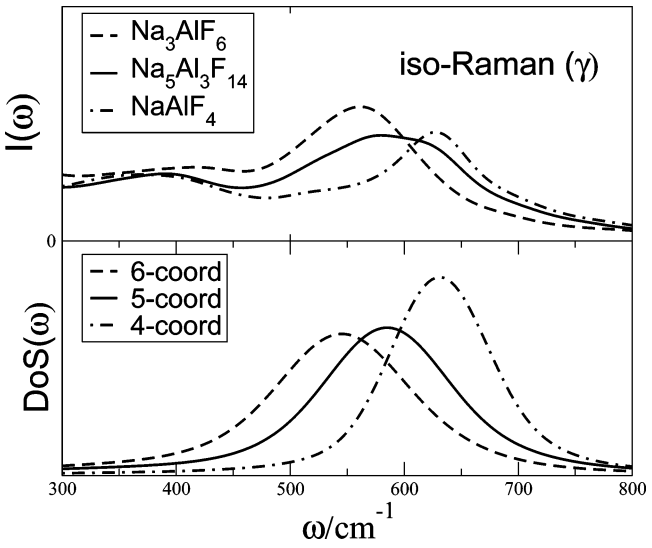

Figure 3. Isotropic Raman spectra (in the top panel) calculated for the γ-hyperpolarizability (SR) mechanism at three different melt compositions compared with the density of states (DoS) of the symmetric breathing vibrations of four-, five-, and six-coordinate complexes.

frequency over a broad range of compositions.[2] The composition dependence of the band in the simulated spectra for the AlF_3/NaF mixtures is *at least* qualitatively similar to that seen in the experimental spectra for these systems. This suggests that the difference between the chloride and fluoride melts seen in the Raman measurements is being picked up by the simulations.

We can examine the association between the structure seen in the main band and the symmetric breathing vibrations of coordination complexes of different nuclearities by appealing to the method introduced by Pavlatou et al.[22] which enables us to extract a separate density of states (DoS) for the symmetric stretching motion of AlF_4^-, AlF_5^{2-}, and AlF_6^{3-} coordination complexes in the melt (see refs 2 and 22). In the lower panel of Figures 2 and 3, we show such densities of states (taken from the simulation at the chiolite composition where, as we will see below, complexes of all three nuclearities are found). It can be seen that the peaks in the densities of states shift to lower frequencies in the sequence $AlF_4^- > AlF_5^{2-} > AlF_6^{3-}$ and that, furthermore, there is a good correspondence between the DoS peaks and the features seen in the Raman bands. In particular, it is tempting to say, from the correspondence of the band positions with the peaks in the DoS, that the SR Raman band for Na_3AlF_6 is dominated by the six-coordinated complex, that for $Na_5Al_3F_{14}$ by the five-coordinate one, and that for $NaAlF_4$ by AlF_4^- vibrations together with a low-frequency shoulder arising from five- and six-coordinate species. The γ spectrum might be described in a similar way, though now at the Na_3AlF_6 composition, the peak is closest to that of the five-coordinate complex, at the chiolite composition, the spectrum appears to be a mixture of four- and five-coordinate vibrations, and in $NaAlF_4$, only the AlF_4^- vibrations are seen. It appears that composition dependence of the spectra of both mechanisms can be interpreted as superpositions of the vibrational bands of the different coordination complexes whose concentrations change with composition as if governed by a chemical equilibrium, but the γ spectra seem to give a higher weighting to the lower coordination structures.

This appealing interpretation, which corresponds well with that applied to the experimental data,[14,15] needs to be treated with some care because it assumes that the vibrational frequencies of the different coordination complexes are themselves

TABLE 1: Peak Frequencies of the Symmetric Stretching DoS Spectra at 1250 K in AlF3/NaF Mixtures[a]

	symmetric stretching modes (cm^{-1})		
AlF_3/NaF mixture	six-coord	five-coord	four-coord
experiment	510	560	622
Na_3AlF_6	545 (545)	579 (579)	628 (634)
$Na_5A1_3F_{14}$	555 (550)	586 (584)	631 (631)
$NaAlF_4$	583 (584)	600 (598)	631 (631)

[a] The values in parentheses correspond to 1350 K.

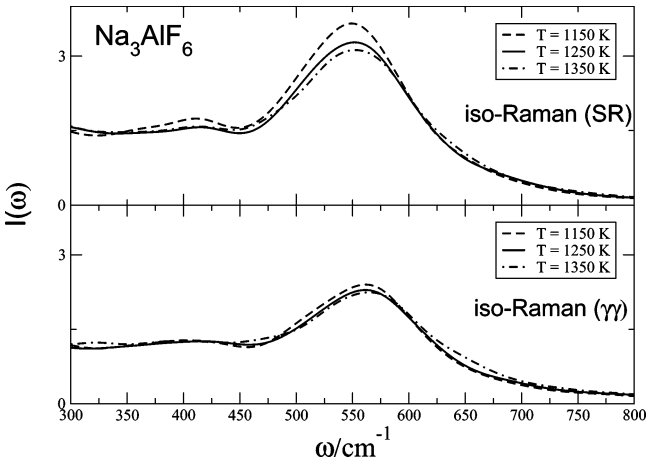

Figure 4. Temperature dependence of the calculated isotropic Raman spectra at the chiolite composition for the short-range and γ mechanisms.

composition independent. In fact, as we show in Table 1, there is some composition dependence in the simulated DoS peak frequencies which, as we shall see, arises because the degree of cross-linking of the coordination complexes changes with composition, with a consequential effect on the symmetric stretching frequencies. Nevertheless, the extent of these composition-dependent shifts is not very large, especially for the AlF_4^- unit, and certainly not large enough to invalidate the overall sense of the interpretation in terms of the vibrations of different coordination structures.

The table also shows that the vibrational frequencies of the symmetric stretching vibrations extracted from the simulations are in surprisingly good accord with those extracted from the experiments (in which it is assumed that these frequencies are composition independent). This is particularly true of the frequencies obtained for the most dilute mixtures.

The interpretation outlined above could be better substantiated if the vibrational DoS bands were somewhat narrower, so that the individual features in the overall Raman spectra were better resolved. Gilbert and co-workers[19] have demonstrated how the resolution can be improved by working at lower temperatures and by working with better "structure-breaking" alkali cations, like Cs^+. In Figure 4, we show the effect of lowering the temperature on the Raman spectrum in the simulations at the cryolite composition. The band can be seen to narrow quite appreciably as the temperature is lowered, suggesting that we could profitably apply these strategies in future work. The results from the different temperatures give a good indication of the statistical quality of the results we have been discussing. Note, in particular, that existence of the weak band at 400 cm^{-1} is confirmed by this comparison. A band is seen in the experimental spectra close to this frequency with a similar intensity relative to the main band as seen in our data.

To complete the discussion of the isotropic spectrum, in Figure 5, we contrast the spectrum for the chiolite composition

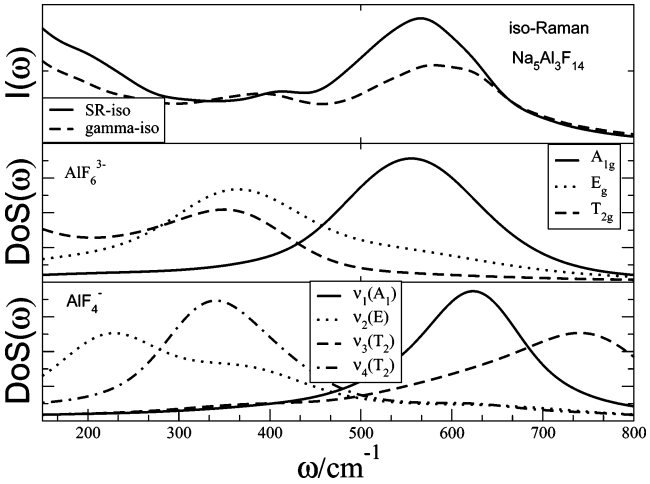

Figure 5. Isotropic SR (full line) and γ (dashed line) subspectra for the mixture $Na_5Al_3F_{14}$. In the other two panels, the DOS spectra for the AlF_6^{3-} and AlF_4^- coordination complexes are shown. Note the approximate correspondence between the weak Raman feature at about 400 cm^{-1} and the modes of the coordination complexes.

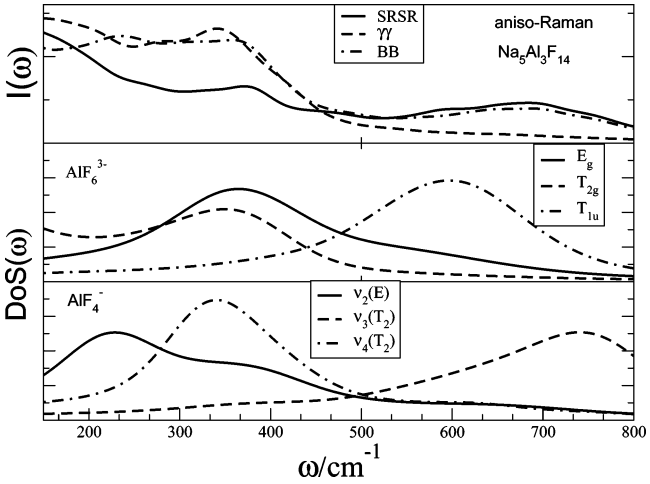

Figure 6. (top) Anisotropic subspectra (SR, full-line; γ, dashed line; *B*-tensor, dot−dashed line) for the $Na_5Al_3F_{14}$ mixture. (middle) Octahedral normal mode vibrational DOS spectra. (bottom) Tetrahedral DOS spectra of the $NaAlF_4$ mixture. The figure suggests associations between the complex vibrations and the bands seen in the depolarized Raman spectra.

with the DoS of the other modes of the coordination complexes in order to examine possible explanations for the 400 cm^{-1} feature. For clarity, we include only those modes which would be Raman active for an isolated complex. We are only able to calculate these nonsymmetric stretch modes for the four- and six-coordinate species; the five-coordinate complex has too low a symmetry to allow the modes to be separated. The comparison shows that the 400 cm^{-1} feature falls in the frequency domain of the E_g and T_{2g} modes of the six-coordinate species and of the T_2-bending modes of the four-coordinate one, though there is not a close correspondence between the DoS peak shapes and the Raman feature. Note that modes of this symmetry cannot contribute to the *isotropic* spectrum of an *isolated* octahedral or tetrahedral molecule; they could only affect the depolarized spectrum. Thus, if the character of the vibrations responsible for the 400 cm^{-1} feature is to be associated with that reflected in the coordination complex normal modes identified above, we note that they only become spectrally active because of the coupling between the vibrations of different complexes through the networklike structure which is illustrated in Figure 1. As such, the fact that there is not a close correspondence between the DoS peaks and the Raman band should be expected. Another possibility, of course, is that a mode of the five-coordinate species is primarily responsible. As we will see below, this is actually the majority species in a melt of this composition. From general considerations of the relationships between the frequencies of normal modes in complexes of different nuclearity,[34] we would expect that the five-coordinate species would have modes of similar mixed stretch−bend character to those of the four- and six-coordinate species which fall in this frequency domain.

B. Depolarized Spectrum. In Figure 6, we illustrate the relationship between the depolarized Raman subspectra calculated at the $Na_5Al_3F_{14}$ composition and the DoS of the normal modes for the four- and six-coordinate species present in the melt. We have omitted the symmetric stretching modes, which would not contribute to the depolarized spectra for isolated complexes. We have shown only three of the Raman subspectra—those corresponding to the SR, γ, and *B*-tensor mechanisms—and the DID spectrum was found to be almost featureless and has been omitted.

All of the subspectra show bands in the 330−380 cm^{-1} frequency range, where the DoS analysis shows E_g and T_{2g} modes of the six-coordinate complex and the T_2(bend) mode of the four-coordinate one are found. Robert et al.[35] report depolarized bands of this character between 320 and 350 cm^{-1} for the different coordination complexes in KF/AlF_3, so this indicates good agreement with experiment for the characteristic frequencies of these motions. Although the correspondence between the Raman and DoS band positions indicates the character of the ionic motion responsible for the Raman feature, it is clear that, due to the width of the Raman band and the fact that several complex vibrations occur in this frequency domain, this depolarized band cannot be used as a diagnostic of coordination structures in the manner of the isotropic band.

The *B*-tensor and SR subspectra show, in addition, a very broad band in the 650−800 cm^{-1} frequency range. This band is centered at higher frequencies than the main band in the isotropic spectra. Robert et al.[35] attribute a weak depolarized feature at 760 cm^{-1} to the AlF_4^- species, so, again, the calculated spectra are reproducing features in accord with experiment. In the DoS analysis, the position of this band corresponds most closely to the range of asymmetric stretching frequencies of the coordination complexes, the T_{1u} mode for the six-coordinate complex and perhaps even more closely with the T_2 mode for the four-coordinate one. Again, we would expect the five-coordinate complex (the majority species at this composition) to have an asymmetric stretching vibration at a frequency somewhere between the six-coordinate and four-coordinate one. The six-coordinate T_{1u} mode is, of course, Raman forbidden for an isolated complex; we include it as a guide to the position of the five-coordinate band but also note that it could become Raman active if the complex were networked as discussed in ref 1.

Robert et al.[35] attribute a depolarized band at 215 cm^{-1} to the AlF_4^- species. Only the *B*-tensor subspectrum shows any distinctive feature in this frequency domain, and gratifyingly, we note that the only DoS which shows a band in this regime is for the *E*-symmetry mode of the four-coordinate species.

V. Structure and Lifetimes of the Coordination Complexes

The above considerations have shown a good degree of consistency between the experimentally observed and simulated

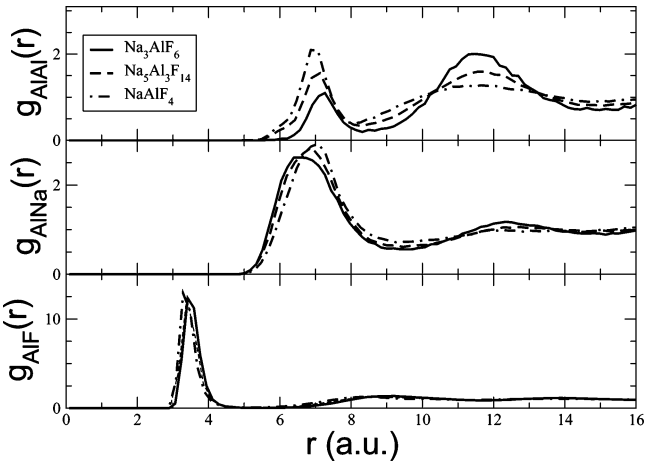

Figure 7. Calculated Al−Al (in the top panel) and Al−Na (in the bottom panel) radial distribution functions in AlF_3/NaF mixtures shown for comparison.

TABLE 2: Distribution of Coordination Numbers in AlF_3/NaF[a]

AlF_3/NaF mixture	Al^{3+} coordination numbers		
	4	5	6
Na_3AlF_6	0.8% (1.52%)	32.53% (34.17%)	66.64% (64.15%)
$Na_5A1_3F_{14}$	10.65% (12.78%)	55.46% (57.49%)	33.87% (29.69%)
$NaAlF_4$	34.83% (35.46%)	48.7% (50.32%)	16.44% (14.2%)

[a] The values in parentheses correspond to 1350 K.

spectra, in particular that the composition dependence of the main bands in the calculated isotropic spectra is similar to that of the experimental one and that it can be ascribed to a shift in the predominance of the differently coordinated species. We can, in a simulation, directly examine these different coordination complexes to provide additional information. Given the similarity of the simulated and experimental spectra, we would hope that this information would be a good guide to the properties of the coordination complexes in the real material.

A. Distribution of Coordination Numbers. We begin by calculating the probability that an Al^{3+} ion has a given number of neighbors at any instant. Neighbors are defined as F^- ions within $r_c = 4.8$ au (the atomic unit of length is the Bohr radius 0.529 18 Å) of the Al^{3+}. This is the position of the minimum of the Al−F radial distribution function illustrated in Figure 7. Given the depth of this minimum, it is clear that the coordination shells are very well-defined and that use of this distance criterion leads to no ambiguity in the assignment of an instantaneous coordination number.

Table 2 shows the percentage of Al^{3+} ions which are four-, five-, or six-coordinate at the different compositions and a temperature of 1250 K. Very few (<0.5%) have coordination numbers outside this range. We also note that the analysis shows *no free fluoride ions*, as sometimes invoked in thermodynamic analyses of the melts; all fluoride ions are found within the neighbor shell of at least one Al^{3+} ion. The table shows that as the composition becomes richer in AlF_3 the mean coordination number moves toward lower values, in accord with the qualitative discussion in the Introduction. At the cryolite (Na_3AlF_6) composition, the predominant species is AlF_6^{3-}, whereas, in $Na_5Al_3F_{14}$ and $NaAlF_4$, it is AlF_5^{2-} with a substantial amount of AlF_4^- in the latter. This analysis directly confirms a shifting equilibrium between the different coordination structure which was invoked in order to explain the concentration dependence of the isotropic Raman band. In brackets, we show the corresponding percentages at 1350 K which indicates a shift to lower coordination numbers with increasing temperature at a given composition.

We note, however, that the relative abundances given in the table do not agree with those deduced from the analysis of the experimental spectrum. In the latter, the five-coordinate species is already the majority species in molten cryolite, and AlF_4^- predominates in $NaAlF_4$.[14,15] This picture is confirmed by the NMR chemical shift studies.[20] The experiments do indicate a shift in the equilibrium composition with temperature which is similar to that we have found. The discrepancy between the experimental findings and the simulation must reflect limitations in the interaction potentials used. It is as if these favor the retention of the higher coordination numbers as the composition becomes AlF_3 rich to a greater degree than the experiments. The potential is good enough to qualitatively recover the composition dependence of the Raman band shapes, but not to reproduce the experimental behavior quantitatively.

B. Linkages between the Coordination Complexes. An important issue to clarify is the extent to which Al^{3+} ions share F^- ions in their coordination shells, thus linking the complexes and ultimately forming an incipient network. As we discussed in the Introduction, the extent of linking is connected to the preferred coordination number. We also expect different degrees of linking to be related to the different behaviors of the isotropic Raman spectra of cryolite and the trivalent metal *chlorides* in which there is extensive network formation at higher concentrations.

An examination of the extent to which Al^{3+} ions share common F^- ions reveals that this is common but that sharing of more than one F^- by the same pair of Al^{3+} ions is very rare. That is, in the language network formers, coordination polyhedra are linked by "corner sharing" rather than by edge or face sharing. We can illustrate the extent of linking by showing, in Figure 7, the Al−Al radial distribution function (rdf) at the three different melt compositions. The figure shows a first peak at about 7 au which is due to Al^{3+} pairs being held together by a bridging F^-; note that this distance is close to twice the position of the first peak in the Al−F rdf (bottom panel). The second broad peak is due to correlations between Al^{3+} ions which are shielded by intact coordination shells. We can see, from the height of the first peak, that the extent of F^- sharing increases as the composition becomes richer in AlF_3; simultaneously, the second peak becomes broader and less well-defined. The figure indicates that, at the cryolite composition, the melt contains mostly unassociated complexes, with the degree of interlinking increasing as we move to $NaAlF_4$. Following the discussion in the Introduction, we can ascribe the discrepancy with experiment on the mean coordination numbers to a tendency of the simulated system to engage in network formation rather than to reduce the coordination number.

The first peak in the Al−Na distributions is prominent and overlaps the position of the first peak in Al−Al. This suggests a competition between the alkali ions and a second Al^{3+} ion bound via a linking F^- ion for the next-neighbor position. It seems clear that alterations in the Na−F interactions could significantly affect the degree of Al−Al linking and therefore also the coordination number.

C. Lifetimes of the Coordination Complexes. Another quantity which is not directly measurable from an experiment is the lifetime of these coordination complexes. A convenient way of characterizing this is the "cage correlation function"[37] which we have used in a number of other simulation studies of molten salts[2,36] as a way to examine the stability of the coordination shell. The cage correlation function detects a

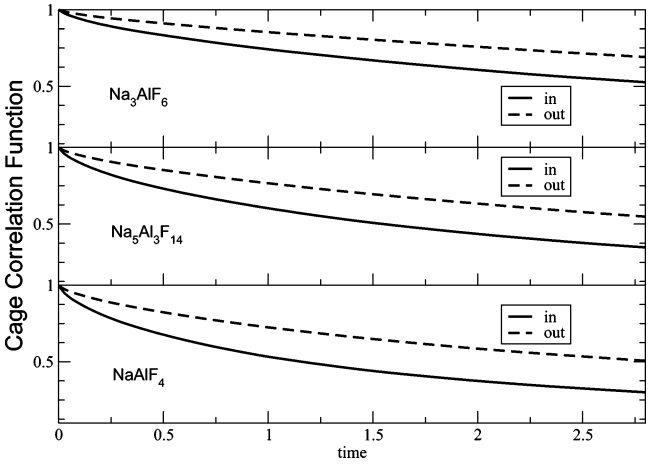

Figure 8. Cage correlation functions (see ref 36 for details) for the Al−F coordination complexes in the AlF_3 and NaF mixtures of various compositions.

change in the identity of any of the ligand ions which are connected to a particular cation. A new anion could enter the coordination shell, which would contribute to the decay of the $C^{in}(t)$ cage correlation function, or an anion could leave, which contributes to the decay of $C^{out}(t)$. The time at which the cage correlation function has decayed to one-half of its original value is the time for half of the complexes to be changed by a change in the identity of one or more ions (or, alternatively, the time over which half of the coordination shells remain intact). A long relaxation time is thus an indicator of stability.

Data for $C^{in}(t)$ and $C^{out}(t)$ for the Al^{3+}-centered coordination complexes in the mixtures of different compositions are shown in Figure 8. It can be seen that the lifetime of the complexes is greatest in the more dilute Na_3AlF_6 mixture where, as we have seen above, the coordination complexes are less likely to be linked together. This parallels the findings on $LaCl_3$/ACl mixtures, where isolated $LaCl_6^{3-}$ complexes in dilute solutions had much longer lifetimes than those involved in intercomplex linkages at higher $LaCl_3$ concentrations.[2] Note too that the typical lifetime of the coordination complexes in the cryolitic melts is of the order of 2.5 ps. This means that the origin of the breadth of the Raman bands (which seems to be of the order of 50 cm^{-1} or more) is *not* lifetime broadening caused by the decomposition of the coordination complexes. Lifetime broadening with a relaxation time of 2.5 ps could account for a contribution of 2 cm^{-1} to the line width. The remaining broadening must arise from an essentially inhomogeneous mechanism, due to the numerous different environments in which the complexes find themselves in this complex structure.

VI. Discussion

We have described calculations of the Raman spectra of NaF/AlF_3 mixtures and have obtained spectra that are similar to those obtained experimentally. Although one might have expected the different mechanisms which contribute to the polarizability fluctuations to have had very different spectral characteristics, this does not seem to be the case; the different subspectra, for the most part, exhibit similar characteristics, and even though we do not know the weights of the different terms, we are able to comment on the origin of the different bands. The band frequencies are in good agreement with experiment in both the isotropic and depolarized spectra, which suggests that the Al−F interactions have been described well by our interaction potentials.

The interesting thing about the results, compared to the previous theoretical Raman spectra studies[1,2] on chlorides, where very similar techniques were used, is that they show a definite change in the position of the main band in the isotropic spectrum as the composition of the melt changes. We have shown how the shift in the character of the band can be associated with changes in the equilibrium between coordination clusters containing four, five, and six F^- ions, as invoked in the explanation of the experimental data.[14,15] The coordination number distribution *does* change with composition in the chloride melts,[2] but the extent of the change is smaller than that for the fluorides and the effect on the Raman spectrum less marked. As we have explained and demonstrated, the response of a melt of this kind to a change in composition involves two effects: a change in coordination number and a change in the degree of cross-linking between coordination complexes. It seems as if the chlorides more readily change the degree of cross-linking with a relatively small change in the preferred coordination number. In the simplest ionic materials, the structure is governed by the ratio of the cation to anion radii;[8,38] in our simulation models, the other parameter which enters is the anion polarizability. Experimental studies of the diffraction patterns exhibited by molten trivalent metal chlorides, bromides, and iodides[39] suggest that the structures of different materials with the same radius ratio are very similar (for example, YCl_3 and $LaBr_3$). Note that this is also true of the crystal structures;[40] the trivalent metal chlorides, bromides, and iodides exhibit the same set of crystal structures with the stability boundaries determined by the ratio of ion size. The similarity of the shapes of the Raman spectra of melts with the same size ratio has also been noted.[16] Since the polarizability plays an important role in the actual structures adopted, we argued that its effect also scaled with the ratio of cation to anion size, within the chlorides, bromides, and iodides, because the polarizability *densities* (i.e., the polarizability divided by the ionic volume) of Cl^-, Br^-, and I^- are very similar.[41] The trivalent metal fluorides do not appear to fall into this common pattern of behavior with the other halides. They exhibit a different set of crystal structures,[40] in which the changes in coordination number (from 6 to 9, etc.) occur at similar radius ratios to the other halides, but the way in which the coordination octahedra are linked together is simpler, resulting in different crystal structures. For example, for smaller radius ratios, the chlorides and fluorides both adopt crystal structures with an octahedral coordination, but the chlorides adopt the layered $AlCl_3$ structure, whereas the fluorides adopt the cubic ReO_3 structure, at least close to melting. As we have discussed above, the behavior of the Raman spectra of the NaF/AlF_3 mixtures is different compared with that of the corresponding chloride (by ion size). From Shannon ionic radii,[42] we might expect the spectra to be similar to those of $ScCl_3$. The changes in the Raman spectrum in $ScCl_3$ on dilution with alkali chlorides are far more extensive and complex[10] than those for larger trivalent cations, but they are not readily related to a shifting equilibrium between simple polyions such as the cryolitic melts. We would speculate that the difference between the properties of the fluorides and other halides is because the fluoride ion polarizability density is lower, resulting in a lower tendency of the fluoride ion to sit in bridging positions between the highly charged cations.

Overall, the work described amounts to a progress report on our effort to calculate Raman spectra from basic principles. We are currently developing new methods to allow the calculation of both the potentials and the polarizability model from purely ab initio considerations. This should bring the work to the point

TABLE 3: SR F^- Polarizability Parameters[a]

ion pair *ij*	σ_{ij}	a_{ij}	c_{ij}	b_{ij}	d_{ij}
F^-−F^-	2.2 + 2.2	0.002 64	1.7693	0.002 64	1.7693
Al^{3+}−F^-	1.1 + 2.2	0.009 41	1.2543	0.006 64	1.7693
Na^+−F^+	1.6 + 2.2	0.004 41	1.254	0.002 64	1.7693

[a] All of the parameters are given in atomic units.

at which it becomes a genuinely diagnostic aid to the interpretation of Raman spectra.

Acknowledgment. Z.A. thanks Queen's College, Oxford for their hospitality during some part of this work and acknowledges support from TUBITAK and from the Research Foundation of Istanbul University under Project No. UDP-485/07062005.

VII. Appendix

A. Parameters for the Polarizability Calculation. The contributions of the short-range mechanism to $\Pi_{\alpha\beta}$ is given by

$$\Pi^{\mathrm{SR}}_{\alpha\beta}(\mathbf{q}) = \sum_i [(\mathbf{K}^i(\{\mathbf{R}^N\}))^{-1}_{\alpha\beta} - \alpha^{i,\mathrm{crys}}\delta_{\alpha\beta}]\mathrm{e}^{i\mathbf{q}\cdot\mathbf{r}^i} \quad (7.1)$$

where $\mathbf{K}^i$ is a tensor (representing the instantaneous value of the force constant matrix of ion *i* in a Drude model of polarizability) which depends on the positions of the neighboring ions

$$\mathbf{K}^i_{\alpha\beta} = (\alpha^{i,0})^{-1}\delta_{\alpha\beta} + \sum_{j\neq i}(f(r^{ij})\delta_{\alpha\beta} + (3\hat{r}^{ij}_\alpha \hat{r}^{ij}_\beta - \delta_{\alpha\beta})g(r^{ij})) \quad (7.2)$$

with *f* and *g* being short-ranged functions of the interionic separation. This form was proposed on the basis of electronic structure calculations of ionic polarizabilities.[4,26]

The functional forms of the SR functions *f* and *g* (eq 7.2) are

$$f(r_{ij}) = a_{ij}\exp[-c_{ij}(r_{ij} - \sigma_{ij})]$$
$$g(r_{ij}) = b_{ij}\exp[-d_{ij}(r_{ij} - \sigma_{ij})] \quad (7.3)$$

where σ_{ij} is the sum of the ion radii of the pair of ions *ij*. A complete parameter set is given in Table 1. The parameters *a*, *b*, *c*, and *d* are as obtained ab initio, for the alkali halides, but the ionic radii σ are taken to be the same as the radii used in the construction of the pair potential, and α^0 for F^- is 8.025 au. Finally, we check that the short-range model gives a reasonable value for the in-crystal polarizability by setting up the AlF_3 system in the (high-symmetry) ReO_3 structure, but with the experimental value of the cation−anion separation in the observed crystal structure, and checking that the mean F^- polarizability obtained from the above expressions is close to the experimental value, deduced from the refractive index. All polarizability model parameter values are given in Table 3.

The remaining contributions to Π are

$$\Pi^{\mathrm{DID}}_{\alpha\beta}(\mathbf{q}) = \sum_i\sum_{j\neq i}\alpha^{i,\mathrm{crys}}\alpha^{j,\mathrm{crys}}T^{ij}_{\alpha\beta}\mathrm{e}^{i\mathbf{q}\cdot\mathbf{r}^i}$$
$$\Pi^{B}_{\alpha\beta}(\mathbf{q}) = \sum_i B^{i,\mathrm{crys}}F'_{\alpha\beta}(\mathbf{r}^i)\mathrm{e}^{i\mathbf{q}\cdot\mathbf{r}^i}$$
$$\Pi^{\gamma}_{\alpha\beta}(\mathbf{q}) = \sum_i \gamma^{i,\mathrm{crys}}F_\alpha(\boldsymbol{r}^i)\,F_\beta(\boldsymbol{r}^i)\mathrm{e}^{i\mathbf{q}\cdot\mathbf{r}^i} \quad (7.4)$$

The time-dependent fluctuations in $\Pi_{\alpha\beta}$ responsible for the spectrum arise from the time dependence of the relative positions of the ions, as reflected in these expressions; the interionic Coulomb field and field gradients F_α and $F'_{\alpha\beta}$ at ion *i* depend on its position with respect to all other ions in the sample. The polarizabilities required to evaluate these expressions were obtained from ab initio calculations on the in-crystal ions.[43,44] $\alpha_F = 6.88$, $\alpha_{Na} = 0.98$, $\alpha_{Al} = 0.192$, $\gamma_F = 283.0$, and $B_F = -54.0$ (all values in atomic units).

TABLE 4: Pair Potential Parameters[a]

ion pair	B_{ij}	α_{ij}	C^6_{ij}	C^8_{ij}	b^6_{ij}	b^8_{ij}
F^-−F^-	30.53	1.63	63.337	777.897	1.6	1.6
$A1^{3+}$−F^-	99.50	2.2	0.0	0.0	2.9	2.9
Na^+−F^-	34.0	1.903	12.061	45.0	1.9	1.9
$A1^{3+}$−AI^{3+}	50.0	2.2	0.0	0.0	1.5	1.0
Na^+−Na^+	11.57	1.603	1.588	0.0	2.9	2.9
Al^{3+}−Na^+	0.0	2.2	0.0	0.0	1.5	1.0

[a] All of the parameters are given in atomic units.

B. Interaction Potential. The interaction potential consists of a pair potential of Born−Mayer form together with an account of interionic polarization.[27] The pair potential is written as

$$V(r_{ij}) = B^{ij}\mathrm{e}^{-\alpha^{ij}r_{ij}} - f^6_{ij}(r_{ij})\frac{C^6_{ij}}{r^6_{ij}} - f^8_{ij}(r_{ij})\frac{C^8_{ij}}{r^8_{ij}} \quad (7.5)$$

where C^6_{ij} and C^8_{ij} are the dispersion coefficients and $f^{(n)}_{ij}$ are dispersion damping functions given by

$$f^{(n)}_{ij}(r_{ij}) = 1 - \mathrm{e}^{-(b^n_{ij}r_{ij})}\sum_{k=0}^{n}\frac{(b^n_{ij}r_{ij})^k}{k!} \quad (7.6)$$

Values for all parameters are given in Table 4. The polarization parts of the potential include fluoride ion polarization only.[5,27] We used a fluoride ion polarizability of 6.88 au and applied a damping function

$$g_{ij}(r_{ij}) = 1 - c_{ij}\mathrm{e}^{-(b_{ij}r_{ij})}\sum_{k=0}^{4}\frac{(b_{ij}r_{ij})^k}{k!} \quad (7.7)$$

to the interaction between the anion dipoles and the cation charges with $b_{FAl} = 1.8$ au^{-1}, $b_{FNa} = 1.8$ au^{-1}, $c_{FAl} = 1.5$, and $c_{FNa} = 1.0$.

References and Notes

(1) Madden, P. A.; Wilson, M.; Hutchinson, F. *J. Chem. Phys.* **2004**, *120*, 6609.
(2) Glover, W. J.; Madden, P. A. *J. Chem. Phys.* **2004**, *121*, 7293.
(3) Madden, P. A.; Board, J.; O'Sullivan, K.; Fowler, P. W. *J. Chem. Phys.* **1991**, *94*, 918.
(4) Madden, P. A.; Board, J. *J. Chem. Soc., Faraday Trans 2* **1987**, *83*, 1891.
(5) Hutchinson, F.; Wilson, M.; Madden, P. A. *Mol. Phys.* **2001**, *99*, 811.
(6) Brooker, H. M., Papatheodorou, G. N., Mamantov, G., Eds. *Advances in Molten Salt Chemistry*; Elsevier: New York, 1983; Vol. 5, p 27.
(7) Tosi, M. P.; Price, D. L.; Saboungi, M.-L. *Annu. Rev. Phys. Chem.* **1993**, *44*, 173.
(8) Rovere, M.; Tosi, M. P. *Rep. Prog. Phys.* **1986**, *49*, 1001.
(9) Photiadis, G. M.; Borresen, B.; Papatheodorou, G. N. *J. Chem. Soc., Faraday Trans.* **1997**, *94*, 2605 and references therein.
(10) Zissi, G. D.; Papatheodorou, G. N. *Chem. Phys. Lett.* **1999**, *308*, 51; *J. Chem. Soc., Dalton. Trans.* **2002**, 2599.
(11) Brookes, R.; Davies, A.; Ketwaroo, G.; Madden, P. A. *J. Phys. Chem. B* **2005**, *109*, 6485.
(12) Grjotheim, K.; Krohn, C.; Malinovsky, M.; Matiasovsky, K.; Thonstad, J. *Aluminium Electrolysis: Fundamentals of the Hall-Hêroult Process*; Aluminium-Verlag: Düsseldorf, Germany, 1982.

(13) Matsuura, H.; Takagi, R.; Zbalocka-Malicka, M.; Rycerz, L.; Szczepaniak, W. *J. Nucl. Sci. Technol.* **1997**, *33*, 895.
(14) Gilbert, B.; Robert, E.; Tixhon, E.; Olsen, J.; Ostvold, T. *Inorg. Chem.* **1996**, *35*, 4198; *J. Phys. Chem. B* **1997**, *101*, 9447.
(15) Gilbert, B.; Materne, T. *Appl. Spectrosc.* **1990**, *44*, 2.
(16) Papatheodorou, G. N.; Yannopoulos, S. N. *Molten Salts: From Fundamentals to Applications*; NATO Science Series II, Vol. 52; Kluwer: Dordrecht, The Netherlands, 2002; p 47.
(17) Papatheodorou, G. N. *Curr. Top. Mater. Sci.* **1982**, *10*, 249.
(18) Brooker, M. H.; Berg, R. W.; von Barner, J. H.; Bjerrum, N. J. *Inorg. Chem.* **2000**, *39*, 3682.
(19) Auguste, F.; Tkatcheva, O.; Mediaas, H.; Ostvold, T.; Gilbert, B. *Inorg. Chem.* **2003**, *42*, 6338.
(20) Lacassagne, V.; Bessada, C.; Florian, P.; Bouvet, S.; Ollivier, B.; Coutures, J. P.; Massiot, D. *J. Phys. Chem. B* **2002**, *106*, 1862.
(21) Robert, E.; Lacassagne, V.; Bessada, C.; Massiot, D.; Gilbert, B.; Coutures, J.-P. *Inorg. Chem.* **1999**, *38*, 214.
(22) Pavlatou, E. A.; Madden, P. A.; Wilson, M. *J. Chem. Phys.* **1997**, *107*, 10446.
(23) Berne, B. J.; Pecora, R. *Dynamic Light Scattering*; Wiley, New York: 1976.
(24) Madden, P. A. In *Liquids, Freezing and the Glass Transition, Les Houches Session LI*; Hansen, J.-P., et al., Eds.; North Holland, Amsterdam: 1991; pp 547−627.
(25) Buckingham, A. D. *Adv. Chem. Phys.* **1967**, *12*, 107.
(26) Fowler, P. W.; Madden, P. A. *Phys. Rev.* **1985**, *B31*, 5443.
(27) Madden, P. A.; Wilson, M. *Chem. Soc. Rev.* **1996**, *25*, 339.
(28) Castiglione, M.; Wilson, M.; Madden, P. A. *Phys. Chem. Chem. Phys.* **1999**, *1*, 165.
(29) Castiglione, M.; Ribeiro, M. C. C.; Wilson, M.; Madden, P. A. *Z. Naturforsch.* **1999**, 54a, 180.
(30) Janz, G. J.; Tomkins, R. P. *J. Phys. Chem. Ref. Data* **1983**, *12*, 659.
(31) Ostvold, T.; Fernandez, R. *Acta Chem. Scand.* **1989**, *43*, 151.
(32) Martyna, G. J.; Tobias, D. J.; Klein, M. L. *J. Chem. Phys.* **1994**, *101*, 5.
(33) Aguado, A.; Madden, P. A. *J. Chem. Phys.* **2003**, *119*, 7471.
(34) Nakamoto, K. *Infrared spectra of inorganic and coordination compounds*; Wiley: New York, 1963.
(35) Robert, E.; Olsen, J. E.; Gilbert, B.; Ostvold, T. *Acta Chem. Scand.* **1997**, *51*, 379.
(36) Morgan, B.; Madden, P. A. *J. Chem. Phys.* **2004**, *120*, 1402.
(37) Rabani, E.; Gezelter, J. D.; Berne, B. J. *J. Chem. Phys.* **1998**, *109*, 4695.
(38) Müller, U. *Inorganic Structural Chemistry*; Wiley: Chichester, U.K., 1993.
(39) Wasse, J. C.; Salmon, P. S.; Delaplane, R. G. *J. Phys.: Condens. Matter* **2000**, *12*, 9539; *Physica B* **2000**, *276*, 433.
(40) Adachi, G., Ed. *Kidorui no Kagaku (Science of Rare Earths)*, Kagaku-dojin, Kyoto, 1999. Page 317 contains a diagram to illustrate this point, taken from the crystal structures in the following: Wyckof, R. W. G. *Crystal Structures*; John Wiley and Sons: New York, 1963; Vols. I−VI. We are grateful to H. Matsuura for bringing this diagram to our attention.
(41) Hutchinson, F.; Wilson, M.; Madden, P. A. *J. Phys.: Condens. Matter* **2000**, *12*, 10389.
(42) Shannon, R. D. *Acta Crystallogr.* **1976**, *A32*, 751.
(43) Fowler, P. W.; Madden, P. A. *Phys. Rev. B* **1984**, *29*, 1035.
(44) Fowler, P. W.; Madden, P. A. *Phys. Rev.* **1985**, *B30*, 6131.